Available online at www.sciencedirect.com
ScienceDirect
Vacuum 82 (2008) 872–879
VACUUM
SURFACE ENGINEERING, SURFACE INSTRUMENTATION & VACUUM TECHNOLOGY
www.elsevier.com/locate/vacuum

Surface erosion and modification by energetic ions

Z. Insepov[a,*], J. Norem[a], D.R. Swenson[b], A. Hassanein[c]

[a]*Argonne National Laboratory, 9700 South Cass Avenue, Argonne, IL 60439, USA*
[b]*Epion Corporation, 37 Manning Road, Billerica, MA 01821, USA*
[c]*Purdue University, 400 Centennial Mall Drive, West Lafayette, IN 47907, USA*

Abstract

Surface erosion and modification by energetic highly charged and cluster ions are important in the development of semiconductor devices, TeV accelerators, fission and fusion reactors, and in the development of extreme ultra-violet lithography devices. Gas cluster ion beam (GCIB) surface treatment can significantly mitigate the high-gradient electric vacuum breakdown of rf-cavities. GCIB can also mitigate Q-slope drop in superconducting Nb-cavities. Various mechanisms of the highly charged ion (HCI) energy transfer into the solid target, such as hollow atom formation, charge screening and neutralization, shock wave generation, and sputtering were analyzed. Surface erosions caused by GCIB, HCI bombardments, and by low energy He^+ and H^+ ions typical for fission and fusion devices were studied by using molecular dynamics simulation. A He bubble splashing mechanism of liquid Li containing was developed, and surface erosion was simulated. The mechanism of bubble explosion could significantly contribute to the surface erosion at high ion fluxes and explain the existing experimental results.
Published by Elsevier Ltd.

Keywords: Molecular dynamics; Gas cluster ion beam; Highly charged ion; Coulomb explosion; Sputtering; Shock wave; Tungsten

1. Introduction

Interactions of energetic ions, such as gas cluster ion beams (GCIB), highly charged ions (HCIs), fission debris, or irradiation of high He^+, H^+ ion fluxes of solid surfaces and bulk materials have fundamental and practical interests in such areas as semiconductor industry [1–7], advanced nuclear fuels [7], fission, fusion reactors, and spallation neutron sources [8], future high-gradient TeV accelerators [9], extreme ultra-violet lithography (EUVL) source development [10], HCI driven SIMS for surface analysis [11], and protein desorption by HCI impacts [12].

Clusters are aggregates which can consist of many weakly bound atoms or molecules. Beams of large clusters can be generated in supersonic expansions of gas into vacuum through a nozzle, ionized by electron bombardment, accelerated and directed toward a target with low energy per atom [1–4]. A unique low energy per atom feature of cluster ion beams has been used for surface smoothing, or, shallow implantation, at ion doses of 10^{13}–10^{15} ions/cm^2 [5].

Development of higher-field rf cavities for future accelerators is restricted by high voltage rf breakdown and Q-drop [9,13]. At an electric field of 25–30 MV/m, a sharp increase of the electron current and an abrupt decrease of the quality factor Q_0 has been observed by many groups (FNAL, CEA, JLab, DESY, KEK). The high-gradient vacuum breakdown is caused by tiny tips of a nanometer size, sharp corners of grain boundaries, foreign atoms, and contaminations that are ideal Fowler-Nordheim sources of the electrons. The Q-slope is attributed to a residual surface resistance (BCS-surface resistance), Kapitza impedance (KI), niobium oxide formation and degradation during baking, and to the Nb grain boundary features.

On the nanoscale there are rather few techniques that can polish surfaces and contaminants to produce surfaces that are smooth enough to be free of field emission and clean enough so that chemical contamination is not a concern. Gas cluster ion beam smoothing, along with a very few other techniques, is one of these options.

*Corresponding author. Tel.: +1 630 252 5049; fax: +1 630 252 3250.
E-mail address: insepov@anl.gov (Z. Insepov).

0042-207X/$ - see front matter Published by Elsevier Ltd.
doi:10.1016/j.vacuum.2007.12.012

While high-pressure water rinsing (HPWR) has been shown to be simple and effective up to a point, many experiments have shown that HPWR cannot produce the best surfaces, in spite of many years of optimization. Therefore, it is necessary to continue to try to develop and optimize GCIB.

Since high field Q slope seems to be a result of surface defects, it is interesting to see if GCIB can be used to mitigate this problem also. These ideas are in a very early stage.

Surface erosion of plasma-facing components (PFC) for future fusion devices is a rapidly expanding area of materials science. The following materials have been studied for the fusion needs: low-Z materials [14], high-Z metals, with high melting point [14–17], and flowing liquid metals [18–21]. Liquid lithium surface is capable of protecting PFC against the fusion plasma [18]. However, there are still fundamental and engineering problems that must be resolved before liquid metals can be used. One of such problems is an enhanced sputtering of the liquid metal surface under high helium and hydrogen plasma ion fluxes. Helium and hydrogen can form bubbles in liquid metals at a certain critical ion flux from the plasma and examining a feasible mechanism of enhanced sputtering due to bubble bursts has attracted much attention [22–26].

Noble fission gases, Xe and Kr, are the main cause of nuclear fuel swelling. Bubble formation in fuels is a very detrimental phenomenon at a high level of burn-up [27]. In nuclear structural materials, helium atoms tend to precipitate into bubbles, resulting in structural changes, degradation of the mechanical properties in fusion and the Generation IV reactors [28,29]; and helium embrittlement in liquid metal reactors [30].

The molecular dynamics (MD) is an ideal method for simulation nano-bubbles and the important radiation effects, such as sputtering and enhanced erosion.

The aim of this paper is to study surface erosion with two types of energetic ions, i.e. Gas cluster ions, HCIs, and with high fluxes of helium ions on liquid lithium surfaces. The following target materials were studied: Nb, which is a material for future accelerators and W, which is a high-Z metal for future fusion device development. Additionally, we examine hydrogen ion collisions with W.

The field emission high-electric field gradient experiments of Nb samples treated with GCIB will be discussed.

2. Simulation models

2.1. Molecular dynamics of energetic ion interaction on a surface

MD has been used to calculate temperature, pressure, and energy of shock waves of various kinds [31–44]. The dynamics of an energetic Ar and oxygen molecular cluster beam impacts on a Nb (0 0 1) surface were examined by a MD method and meso-scale surface dynamics equations. The boundary conditions were used as in our previous work [45]. Our MD method combines conventional atomistic MD, for the central cluster collisional zone, with a continuum mechanics representation, for the rest of a system. It significantly reduces the system size and can keep the accuracy of the energy flow through the system boundaries.

Temperature, pressure, energy, stress tensor, and the velocity of moving matter within a spherical layer were calculated [31,32,46]. A shock wave front in an ideal non-viscous and non-thermal conductive gas is a zero-thickness surface which moves with a hypersonic velocity [47]. The front of this rise has been considered as a shock wave front.

The lateral-sputtering effect (LSE) that was predicted by MD in [2] is a new physical effect that occurs at a surface bombarded with large energetic cluster ions. LSE can be explained by interaction of a strong rarefaction shock wave initiated by a cluster beam impact with an open surface [1–5,47].

2.2. Highly charged ion collision on a surface

As an HCI ion approaches a metal or semiconductor surface, the strong Coulomb field of HCI can pull the electrons from the solid surface into the Rydberg states of the ion and form a hollow atom (HA) [48,50,51]. The HA evolves further by emitting electrons and/or photons via the Auger processes. The potential energy of Xe^{+q} ($q \leqslant 54$) is calculated by a multi-configuration Dirac–Fock method [49]. The total energy of HCI is roughly equal to the total ionization energy: $E_{pi} = qI_{Xe}$, where q is the charge state.

The total energy of the HCI system after the collision with the surface is mainly defined by Coulomb interaction between charges. An electric field screening length of the order of the lattice parameter was used in most of the HCI-surface collision simulations [52,53].

The excessive charge inserted into a surface is eventually neutralized with the times that can be associated with the Maxwell relaxation time: $N_q(t) = N(0)\exp(-t/\tau)$, where $\tau = \varepsilon\varepsilon_0/\sigma$. Here, $N_q(t)$ is the total number of charges at a time t. ε and ε_0 are the electrical permittivity of a material and vacuum, respectively. This allows one to find the neutralization times from the fundamental material

Table 1
Neutralization times of various materials obtained from the Maxwell relaxation formula given in the text

Materials	Conductivity $(\Omega\,m)^{-1}$	Neutralization time τ (fs)
Au	4.55×10^7	0.02
W	1.89×10^7	0.1
Si	100	10^3
LiF	10^{-4}	10^9
GaAs[a]	2.8×10^{-6}	10^{10-11}

[a]Although GaAs is a semiconductor, its intrinsic carrier density at 300 K is very low: $n_i = 2 \times 10^7\,cm^{-3}$. Therefore, the conductivity of pure GaAs is extremely small.

properties. Table 1 shows the neutralization times calculated for various materials.

2.3. Surface erosion of solid targets

MD models of surface sputtering were developed for Si, Li, W, and Nb. Clusters were built of Ar atoms and O_2 molecules interacting via the Buckingham potential; and Nb (1 0 0) and W (1 0 0) surface atoms were interacting via Embedded-Atom-Method-potentials. The Stillinger–Weber and Born–Mayer potential functions were used for Si [54,55], and Finnis-Sinclair potentials for W, Nb [56]. Interactions between H^+ ions and W target atoms were modelled via a Tersoff potential developed in [14]. The potential functions for Li–Li and helium–Li interactions are given in the next sub-section.

The surface slab was bombarded by gas clusters, HCIs, or singly charged helium and hydrogen ions. The size of the clusters was chosen to be 429 atoms/molecules and the HCI types were Xe^{+q} ($q = 8$–44). The total number of target atoms was about 400,000 for energy of 50–100 eV/atom, and the total cluster energy of about 30 keV.

N_q ions were placed into a surface hemi-sphere, and the total potential energy of ions (U_q) plus the ionization energy of N_q ions were equated to the total potential energy of the incident Xe^{q+} (Epi).

The sputtering yields were obtained as a long-time limit of a function $y(t)$ which represents the total number of atoms that crossed a certain control plane above the surface, as a function of the potential energy of Xe^{q+}.

Damage to the target caused by energetic ion impacts was studied by calculating local variables, such as temperature, density, hydrodynamic pressure, shear and normal stresses, the coordination number, the slip vector, and the symmetry parameter of the local environment for each atom [6,57].

2.4. Surface erosion via helium bubble splashing

Surface erosion of liquid Li were studied by MD. Two different types of effective inter-ionic potential for liquid Li were used for this work. The first potential was developed in [58] for five temperatures: 470, 525, 574, 725, 843 K, and corresponding densities along the melting line. The second Li–Li potential is given in an analytic form in [59]. Li–He interactions were modelled by using a potential between Li ions and He atoms given in [60], and He–He interaction was determined via a simple pair-wise potential, with the binding energy and the equilibrium distance from [61].

Helium bubbles were formed in liquid lithium, equilibrated near the open surface, and then released. The imbalanced pressure pushes the bubbles out of the lithium into the vacuum. The sputtering coefficient was obtained as a number of Li atoms per helium atom that were sputtered in the bubble burst.

2.5. Mesoscale surface modification equations

A mixed continuum-discrete model will be used for surface modification in which each HCI or GCIB impact instantly creates a hemi-spherical symmetrical crater and a rim around it. The crater volume and the volume of the rim parameters of the model depending on the impact energy. The total number of atoms leaving surface is higher than the number of redepositing atoms; therefore, the surface height is decreasing with time. The mesoscale surface dynamics equation represents the nonlinear dynamics of growing surface profiles in terms of the coarse-grained interface heights $h(\boldsymbol{r},t)$ in a d-dimensional space where $\boldsymbol{r}$ is the radius-vector in a $(d-1)$-dimensional plane at time t, and accurately describes behaviour in later-stages, or scaling properties, of a growing interface and can be found elsewhere [13].

3. Simulation results

3.1. HCI interaction with Si and W

Our calculations were compared with the experimental sputtering yields obtained for Si, Al, Cu, Ni [49], and LiF, SiO_2, GaAs [49,62,63]. The W sputtering yields were calculated for various neutralization times $\tau_n = 0.1$–1000 fs. The results for Xe^{+q} ($q \leqslant 44$) sputtering of Si (1 0 0) and W (1 0 0) surfaces are shown in Fig. 1. As the Si experimental yield is given in relative units [49], our comparison shows a good agreement of the calculated slope. For W neutralization times $\tau_n < 15$ fs, there are two characteristic energy regions where the yields have a small slope, and a higher, approximately 3/2 power-law dependence, above the threshold.

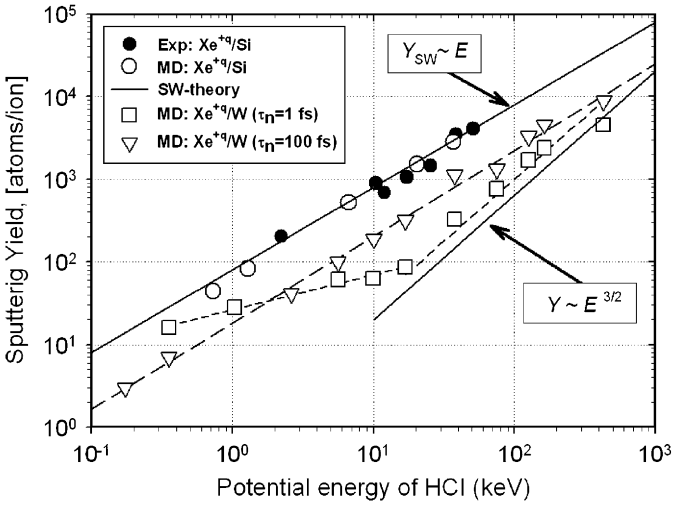

Fig. 1. Comparison of calculated sputtering yield of Xe^{+q} ($q \leqslant 44$) on Si (1 0 0) and W (1 0 0) surfaces with experimental data for Si [49]. The dashes are linear fits to the data points and MD data. The W yields are shown for two neutralization times: $\tau_n = 0.1$ and 100 fs. The solid lines are drawn according to a simple shock-wave theory model [47] and as a 3/2 power law.

Shock wave generation was studied for a Xe^{+44} HCI impact on a Si (1 0 0) surface. The upper solid line in Fig. 1 is drawn according to a simple shock-wave theory model [47] which predicts a linear dependence of the sputtering yield on the total Coulomb energy.

The velocity distribution of the ejected atoms reveals the mechanism of sputtering: the shock wave mechanism gives a v^{-3} dependence at higher velocities which can be obtained from the shock wave theory [45,47].

3.2. GCIB interaction with Nb surface

Crater shapes were studied by MD simulation of an Ar_{429} cluster with the kinetic energy of 125 eV/atom, a $(O2)_{429}$ cluster with energy of 50 eV/mol on a Nb (1 0 0), Xe^{+q} ($q \leqslant 44$) on a W (1 0 0) surface. A preliminary analysis based on the local atomic stresses [6] and on the slip vector calculation [57] showed that both the GCIB and HCI craters strongly emit dislocation loops and stacking faults that are located near the surface. The calculated shear stress for the W was well above the lattice strength and the W bulk modulus [65]. Such extended defects can easily be the driving force for the surface hillocks observed on the conductive surfaces irradiated by HCI ions [66–68].

We modelled surface modification of a Nb surface containing two types of surface tips, with greatly different sizes: one of the tips was a narrow and tall hill, with the diameter of a few nm, and the second tip was modelled with a wide and short hill having a typical area of a many tens of nm. Both of these tips had equal volumes and are

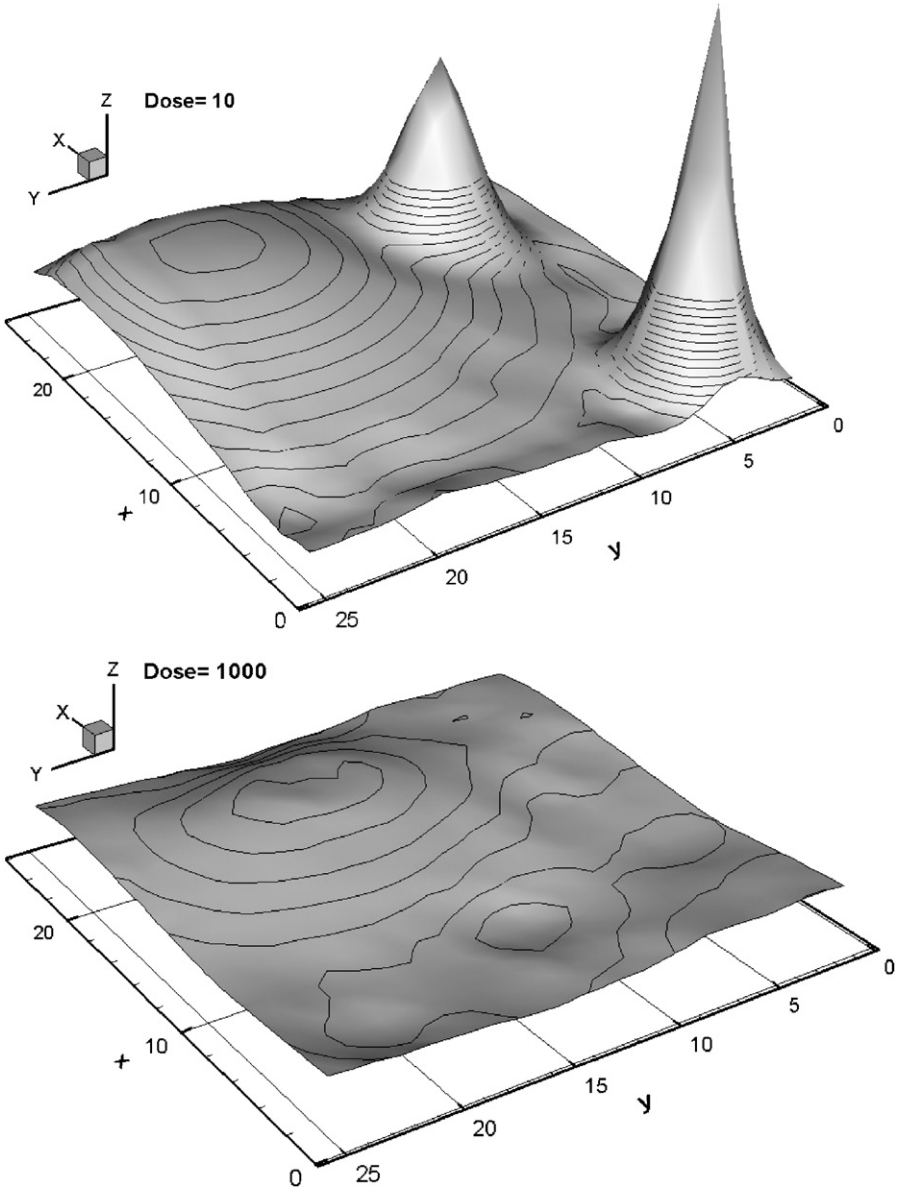

Fig. 2. The results of a mesoscale simulation for the Nb surface smoothening irradiated by O_2 molecular cluster ion beam at a maximum dose of 10^{13} ions/cm^2. The cluster energy was 30 keV and the cluster size was of about 3000 oxygen molecules in a cluster. The surface contained two types of tips: narrow and tall and wide and short.

shown in Fig. 2. The total modelled area was in the order of 10^6–10^7 Å^2, and this area was irradiated by up to 1000 large oxygen 30 keV clusters bombarded randomly the whole simulation cell. The cluster dose was in the order of 10^3–10^4 cluster/cell. Fig. 2 demonstrates the results of our simulations for the Nb surface smoothening. The simulation showed that the narrower hill is removed by an irradiation dose that is five times lower than for the blunt hill. The narrower hills have a higher chemical potential than those with a larger diameter. Therefore the surface treatment by chemically inactive GCIB should remove narrow hills faster than the bigger ones.

3.3. Surface erosion of W by low energy hydrogen ions

Sputtering yield calculations at light ion energies below 100 eV are sparse and they are very time consuming, since the sputtering coefficients are of the order of 10^{-3}–10^{-5}. There are a few studies that have calculated the sputtering yield of hydrogen ions on a W surface [14]. Fig. 3 presents a comparison of the sputtering yields and reflection coefficients of H^+ ions bombarding a W (1 0 0) surface, calculated in the present work, with the experiments [17,69] for H^+/W and D^+/W collisions. The TRIM yield is given as a solid line. The reflection coefficients of H^+ ions and a single sputtering yield data point at 600 eV calculated in [14] are also shown for comparison.

3.4. Sputtering yield of liquid lithium surface via helium bubble splashing

Fig. 4 shows our calculated results for the bubble splashing mechanism calculated at $T = 500$ K for the

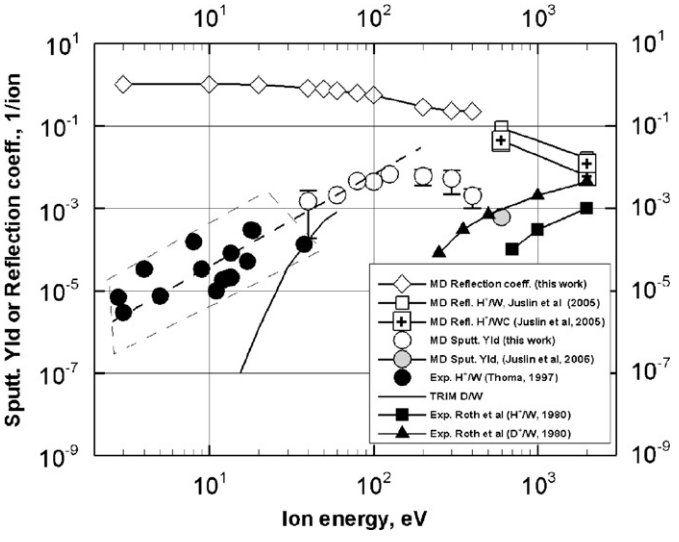

Fig. 3. Comparison of the sputtering yields and reflection coefficient of H^+ ions on a W (1 0 0) surface calculated in present work (open circles and open diamonds) with experimental data of Thoma et al. [17]—solid circles and Roth et al. [69]—solid triangles (H^+/W), solid squares (D^+/W), TRIM and with the reflection coefficients calculated by MD in [14] (open circles, circles with crosses), and a single calculated sputtering yield data point (gray diamond) at 600 eV [14].

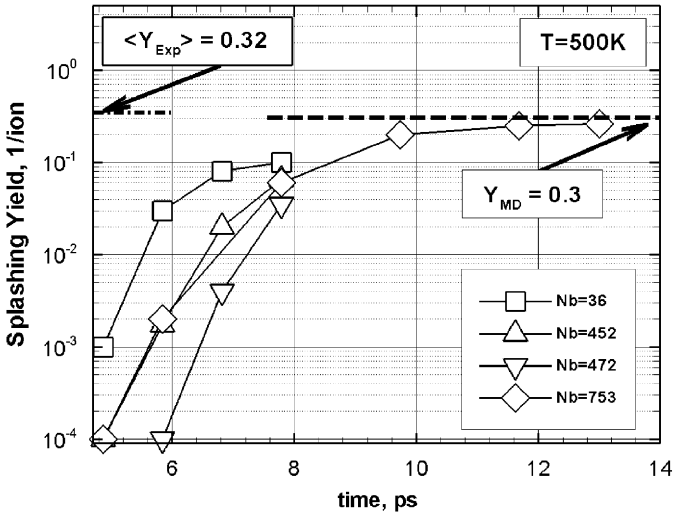

Fig. 4. He splashing yields at $T = 500$ K at various times from the start of bubble burst due to interaction of bubble with an open lithium surface. The results correspond to the following bubble sizes: $N_b = 36$, 452, 472, and 753 helium atoms in the bubble. MD gives the prediction for the sputtering yield of $Y = 0.3$, close to the experimental value of $Y = 0.32$ obtained in [26] for a liquid alloy S-GIO at 653 K, and is shown by an arrow at the left.

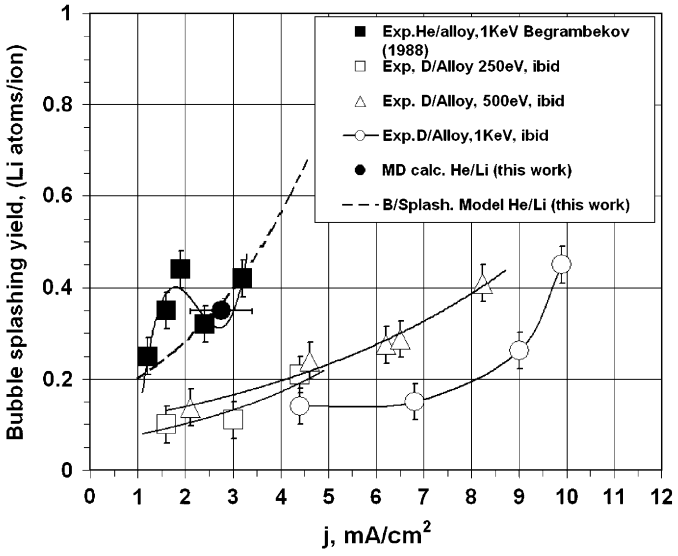

Fig. 5. Lithium splashing yields due to the bubble splashing mechanism calculated by MD (closed circle); dash line is drawn by using a simple model; these two results can be compared with the experimental results on enhanced erosion of a liquid alloy surface irradiated with He^+ (closed squares), and deuterium ions (open triangles and circles) [26].

following helium bubble sizes: $N_b = 36$, 452, 472, and 753. A single experimental data point $\langle Y \rangle \approx 0.32$ was obtained for a S-GIO alloy[1] at $T = 653$ K, and it is shown by an arrow at the left axis [26]. A theoretical prediction for the yield of $Y_{MD} \approx 0.3$ is shown by an arrow at the right axis.

[1] 67% gallium, 20.5% indium, 12.5% tin.

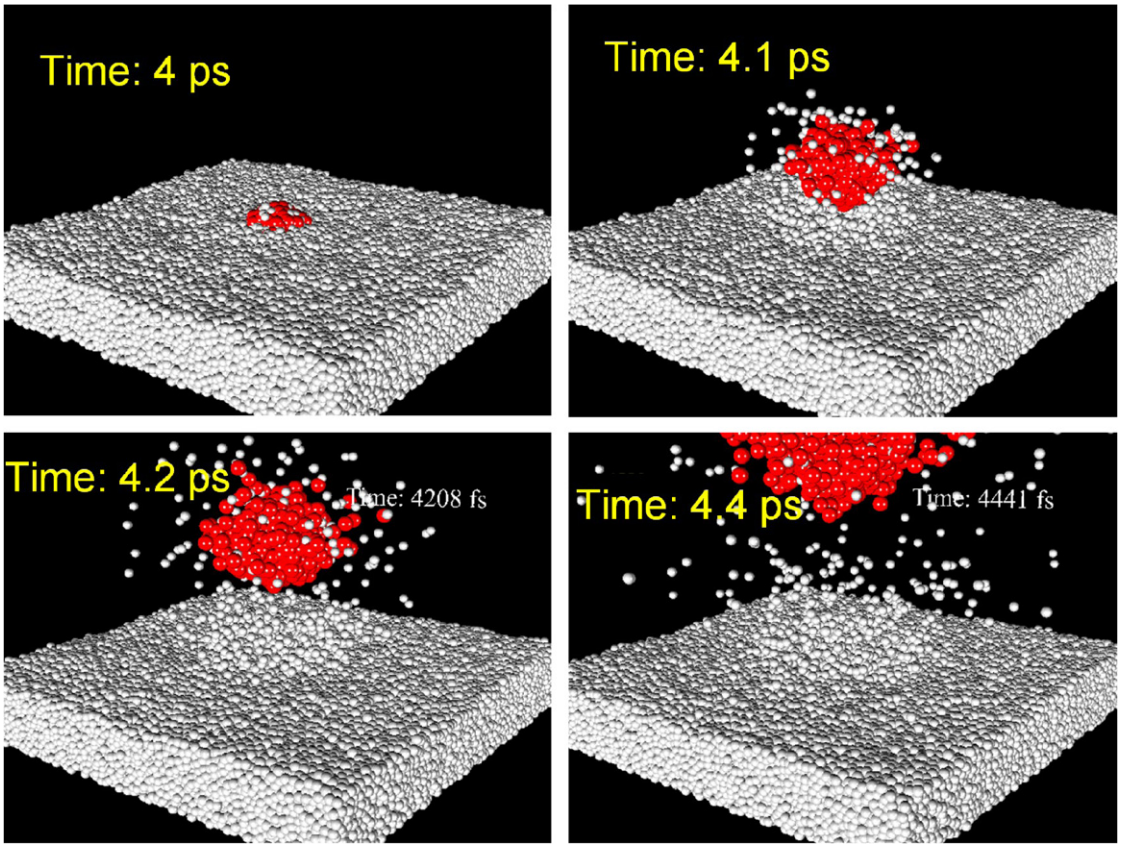

Fig. 6. Bubble explosion that occurs when liquid lithium faces fusion plasma with a high flux of helium and hydrogen ions and lithium becomes saturated with helium or hydrogen ions.

In Fig. 5, the bubble splashing yield calculated by MD is compared with the experimental results [26] on enhanced erosion of a liquid alloy surface irradiated with He^+ and D^+ ions. The dashed line is drawn according to a simple model that uses the time dependence of the bubble radius obtained in [26], which shows a qualitative ion flux dependence of the yield.

Fig. 6 shows an overall picture of bubble explosion that occurs when liquid lithium faces fusion plasma with a high flux of helium and hydrogen ions, and liquid lithium is saturated with helium or hydrogen ions.

4. Experimental

Recent work by EPION Corp, collaborating with Argonne, JLab, Fermilab, and Cornell has demonstrated that GCIB is one of the few options which might be able to make a significant difference in International Linear Collider costs and operation. While the GCIB tests done so far have not been definitive, they have left people optimistic that better results are possible [64].

The field emission of a 150-mm diameter stainless steel electrode was measured at the Jefferson Laboratory Large Area Electrode Test Chamber as a function of the gap field. This electrode was treated using a sequence of high and then low energy Ar, for smoothing followed by high and then low energy O_2 to improve the oxide characteristics.

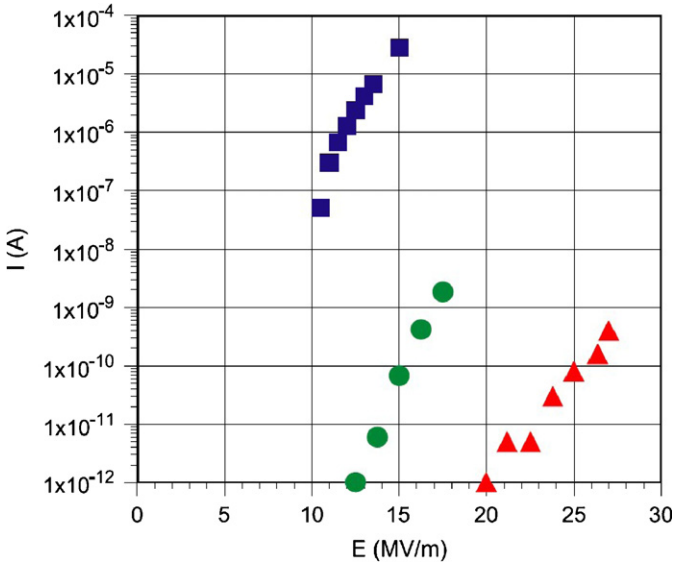

Fig. 7. Field emission current as a function of applied gradient for a 150-mm-diameter stainless steel electrodes: (squares) a typical untreated sample, (circles) first measurement of GCIB treated sample, (triangles) remeasurement of GCIB treated sample after high-voltage conditioning [70].

Fig. 7 shows a comparison of this electrode to a typical non-processed electrode. The GCIB processing caused a reduction of six orders of magnitude in the field emission.

This same electrode was re-measured several months later at Cornell Wilson Laboratory and a gradient of over 20 MV/m was reached with no measurable field emission, as plotted in Fig. 7 [70]. It should also be noted that the processing of this electrode included treatments with O_2 clusters which increased the thickness of surface oxide layer from 1.5 to >10 nm.[2] The treated surface was also measured to be twice as hard as the untreated surface.[2]

5. Summary

Various mechanisms of surface erosion by GCIB and HCI ion bombardments were studied by MD: shock wave generation, crater formation, and sputtering of Si (1 0 0) and W (1 0 0) surfaces irradiated by highly charges slow Xe^{+q} ions, and bubble splashing mechanism. The calculated sputtering yield slope of Si surfaces bombarded by highly charged Xe^{+q} ions show a good agreement with existing experiment. A preliminary analysis of the stresses and dislocation emission from the impacts of HCI and accelerated clusters has been conducted.

Surface modification of Nb surfaces with gas cluster ion beams (GCIB) has been proposed as a means for controlling the microstructure of superconducting rf cavity surfaces. The results of the smoothing experiments show the reduction of the dark current by a factor of 10^6.

Surface erosion of a liquid metal by a new bubble explosion mechanism at high helium ion fluxes typical for fusion reactor conditions were simulated by MD.

Acknowledgments

This work was supported in part by Contract DE-FG02-04ER83944 with Epion Co. and in part by the US Dept. of Energy under Contract W-31-109-Eng-38.

References

[1] Yamada I, Brown WL, Northby JA, Sosnowski M. Nucl Instr Meth Phys Res B 1993;99:223–6.
[2] Insepov Z, Sosnowski M, Yamada I. In: Yamada I, et al., editors. Laser and Ion Beam Modification of Materials. Amsterdam: Elsevier; 1994. p. 111–8.
[3] Yamada I, Matsuo J, Insepov Z, Akizuki M. Nucl Instr Meth Phys Res B 1995;106:165–9.
[4] Yamada I, Matsuo J. In: Tu KN, Mayer JWQ, Poate JM, Chen LJ, editors. Materials research society symposium proceedings, vol. 427. Advanced Metallization for Future ULSI; 1996. p. 263.
[5] Yamada I. In: Kirkby KJ, Gwilliam RM, Smith A, Chivers D, editors. Proceedings of the 16th international conference on ion implantation technology (IIT 2006), Marseille, France. AIP Conference Proceedings, vol. 866; 2006. p. 147–54.
[6] Haberland H, Insepov Z, Moseler M. Phys Rev B 1995;51:11061–7.
[7] Olander DR. Fundamental aspects of nuclear reactor fuel elements. NTIS, US Department of Commerce; 1976. VA: Springfield.
[8] Mansur LK, Rowcliffe AF, Nanstad RK, Zinkle SJ, Corwin WR, Stoller RE. J Nucl Mater 2004;329–333:166–72.
[9] Norem J, Insepov Z, Konkashbaev I. Nucl Instr Meth A 2005;537:510–20.
[10] Allain JP, Hassanein A, Burtseva T, Yacout A, Insepov Z, Taj S, et al. SPIE Proc 2004;5374:112–21.
[11] Hamza A, Schenkel T, Barnes A, Schneider D. US Patent no. 6,261,820 B1, 18 September 2001.
[12] Ruehlicke C, Schneider D, Schneider M, DuBois RD, Balhorn R. Nanotechnology 1998;9:251–6.
[13] Insepov Z, Hassanein A, Norem J, Swenson DR. Nucl Instr Meth Phys Res B 2007;261:664–8.
[14] Juslin N, Erhart P, Träskelin P, Nord J, Henriksson KOE, Nordlund K, et al. J Appl Phys 2005;98:123520.
[15] Causey RA, Venhaus TJ. Phys Scr 2001;T94:9–15.
[16] Hirai T, Rubel M, Philipps V, Huber A, Tanabe T, Wada M, et al. Phys Scr 2003;T103:59–62.
[17] Thoma A, Asmussen K, Dux R, Krieger K, Herrmann A, Napiontek B, et al. ASDEX Upgrade Team Plasma Phys Control Fusion 1997;39:1487–99.
[18] Majeski R, Doerner R, Kaita R, Antar G, Timberlake J, Spaleta J, et al. Prinston Plasma Physics Laboratory, preprint PPPL-3509; 2000.
[19] Doerner RP, Baldwin MJ, Krasheninnikov SI, Whyte DG. J Nucl Mater 2003;313–316:383–7.
[20] Allain JP, Coventry MD, Ruzic DN. J Nucl Mater 2003; 313–316:641–5.
[21] Allain JP, Brooks JN, Alman DA, Gonzalez LE. J Nucl Mater 2005;337–339:94–8.
[22] Hassanein A. Laser Particle Beams 2000;18:611–22.
[23] Medin S, Basko M, Churazov M, et al. Nucl Instr Meth Phys Res A 2005;544:300–9.
[24] Insepov Z, Hassanein A. J Nucl Mater 2005;337–339:912–6.
[25] Bazhirov TT, Norman GE, Stegailov VV. Doklady Phys 2005;50: 570–6.
[26] Begrambekov LB, Zakharov AM, Pustobaev AA, Tel'kovskii VG. Transl From At Energ 1988;64:212–5.
[27] Hoffman G, Kim YS. Nucl Eng Technol 2005;37:299–308.
[28] Suzudo T, Kaburaki H, Wakai E. In: Joint international topics meeting on mathematics and computation and supercomputing in nuclear applications (M&C + SNA 2007), Monterey, CA; April 15–19, 2007. American Nuclear Society, LaGrange Park, IL; 2007.
[29] Mansur LK, Rowcliffe AF, Nanstad RK, Zinkle SJ, Corwin WR, Stoller RE. J Nucl Mater 2004;329–333:166–72.
[30] Garner FA. In: Cahn RW, Haasen P, Kramer EJ, editors. Materials science and technology—a comprehensive treatment, 10A, nuclear materials, Part I; 1994. p. 419–543.
[31] Paskin A, Dienes GJ. J Appl Phys 1972;43:1605–10.
[32] Klimenko VYu, Dremin AN. Sov Phys Dokl 1980;25:288.
[33] Holian BL, Hoover WG, Moran B, Straub GK. Phys Rev A 1980; 22:2798–808.
[34] Holian BL. Shock waves and spallation by molecular dynamics. In: Mareschal M, Holian BL, editors. Microscopic simulations of complex hydrodynamic phenomena, NATO ASI series B, vol. 292. New York: Plenum Press. p. 75–85.
[35] Webb RP, Harrison Jr. DE. Appl Phys Lett 1981;39:311–2.
[36] Even U, Shek I, Jortner J. Chem Phys Lett 1993;202:303.
[37] Insepov Z, Yamada I. Nucl Instr Meth Phys Res B 1996;112:16–22.
[38] Aderjan R, Urbassek HM. Nucl Instr Meth Phys Res B 2000; 164&165:697–704.
[39] Anders C, Urbassek HM, Johnson RE. Phys Rev B 2004;70:155404.
[40] Bringa EM, Johnson RE. Nucl Instr Meth Phys Res B 1998; 143:513–35.
[41] Bringa EM, Johnson RE, Dutkiewicz L. Nucl Instr Meth Phys Res B 1999;152:267–90.
[42] Bringa EM, Nordlund K, Keinonen J. Phys Rev B 2001;64: 235426.
[43] Bringa EM, Johnson RE, Papaleo RM. Phys Rev B 2002;65: 094113.
[44] Jakas MM, Bringa EM, Johnson RE. Phys Rev B 2002;65:165425.

[2] C.K. Sinclair, private communication.

[45] Insepov Z, Yamada I. Nucl Instr Meth Phys Res B 1997;121:44–8; Insepov Z, Manory R, Matsuo J, Yamada I. Phys Rev B 2000;60: 8744–52.
[46] Verlet L. Phys Rev 1967;159:98–103; Egami E, Maeda K, Vitek V. Philos Mag 1980;41:883–901.
[47] Zel'dovich YB, Raizer YP. Physics of shock waves and high temperature hydrodynamic phenomena. New York: Academic Press; 1967.
[48] Burgdörfer J, Lerner P, Meyer FW. Phys Rev A 1991;44: 5674–85.
[49] Sekioka T, Terasawa M, Mitamura T, Stockli MP, Lehnert U, Fehrenbach C. Nucl Instr Meth B 2001;182:121–6.
[50] Burgdörfer J. In: Lin CD, editor. Fundamental processes and applications of atoms and ions. Singapore: World Scientific; 1993. p. 517.
[51] Tökési K, Wirtz L, Lemell C, Burgdörfer J. Phys Rev A 2001; 64:0429021.
[52] Bringa EM, Johnson RE. Phys Rev Lett 2002;88:165501.
[53] Bringa EM. Nucl Instr Meth B 2003;209:1–8.
[54] Stillinger FN, Weber TA. Phys Rev B 1985;31:5262–71.
[55] Woodcock LV, Angell CA, Cheesemann P. J Chem Phys 1976; 65:1565–77.
[56] Finnis M, Sinclair J. Philos Mag A 1984;50:45–55; Ackland GJ, Thetford R. Philos Mag A 1987;56:15–30.
[57] Kelchner CL, Plimpton SJ, Hamilton JC. Phys Rev B 1998;58:11085; Zimmerman JA, Kelchner CL, Klein PA, Hamilton JC, Foiles SM. Phys Rev Lett 2001;87:165507.
[58] Canales M, Gonzalez LE, Padro JA. Phys Rev E 1994;50:3656–69.
[59] Li Y, Blaisten-Barojas E, Papaconstantopoulos DA. Phys Rev B 1998;57:15519.
[60] Soldan P, Lee EPF, Lozeille J, Murrell JN, Wright TG. Chem Phys Lett 2001;343:429–36.
[61] Aziz R, Slaman MJ. J Chem Phys 1991;94:8047–53.
[62] Aumayr F, Varga P, Winter HP. Int J Mass Spectr 1999;192:415–24.
[63] Schenkel T, Barnes AV, Hamza AV, Banks JC, Doyle BL, Schneider DH. Phys Rev Lett 1998;81:2590–3.
[64] Swenson DR, Degenkolb E, Insepov E. Physica C 2006;441:75–8.
[65] Roundy D, Krenn CR, Cohen ML, Morris Jr. JW. Philos Mag A 2001;81:1725–47.
[66] Gebershuber IC, Cerusca S, Aumayr F, Winter HP. Nucl Instr Meth B 2003;205:751–7.
[67] Gebershuber IC, Cerusca S, Aumayr F, Winter HP. Int J Mass Spectr 2003;229:27–34.
[68] Skuratov VA, Zinkle SJ, Efimov AE, Havancsak K. Surf Coat Technol 2005;196:56–62.
[69] Roth J, Bohdansky J, Martinelli AP. Rad Effects 1980;48:213–20.
[70] Swenson DR, Wu AT, Degenkolb E, Insepov Z. Nucl Instr Meth Phys Res B 2007;261:630–3.